Takahiro Numai

Fundamentals of Semiconductor Lasers

With 166 Figures

Springer

Professor Takahiro Numai
Department of Electrical
and Electronic Engineering
Ritsumeikan University
1-1-1 Noji-Higashi, Kusatsu
Shiga 525-8577
Japan
numai@se.ritsumei.ac.jp

Library of Congress Cataloging-in-Publication Data
Numai, Takahiro.
Fundamentals of semiconductor lasers / Takahiro Numai.
p. cm. – (Springer series in optical sciences ; v. 93)
Includes bibliographical references and index.
ISBN 0-387-40836-3 (alk. paper)
1. Semiconductor lasers. I. Title. II. Series.
TA1700.N86 2004
621.36'6–dc22 2003060811

ISBN 0-387-40836-3 ISSN 0342-4111 Printed on acid-free paper.

Printed in the United States of America.

9 8 7 6 5 4 3 2 1 SPIN 10944981

www.springer-ny.com

Springer-Verlag New York Berlin Heidelberg
A member of BertelsmannSpringer Science+Business Media GmbH

Preface

Semiconductor lasers have been actively studied since the first laser oscillation in 1962. Through continuing efforts based on physics, characteristics of semiconductor lasers have been extensively improved. As a result, they are now widely used. For example, they are used as the light sources for bar-code readers, compact discs (CDs), CD-ROMs, magneto-optical discs (MOs), digital video discs (DVDs), DVD-ROMs, laser printers, lightwave communication systems, and pumping sources of solid-state lasers. From these facts, it may be said that semiconductor lasers are indispensable for our contemporary life.

This textbook explains the physics and fundamental characteristics of semiconductor lasers with regard to system applications. It is aimed at senior undergraduates, graduate students, engineers, and researchers. The features of this book are as follows:

1. The required knowledge to read this book is electromagnetism and introductory quantum mechanics taught in undergraduate courses. After reading this book, students will be able to understand journal papers on semiconductor lasers without difficulty.
2. To solve problems in semiconductor lasers, sometimes opposite approaches are adopted according to system applications. These approaches are compared and explained.
3. In the research of semiconductor lasers, many ideas have been proposed and tested. Some ideas persist, and others have faded out. These ideas are compared and the key points of the persisting technologies will be revealed.
4. The operating principles are often the same, although the structures seem to be different. These common concepts are essential and important; they allow us to deeply understand the physics of semiconductor lasers. Therefore, common concepts are emphasized in several examples, which will lead to both a qualitative and a quantitative understanding of semiconductor lasers.

This book consists of two parts. The first part, Chapters 1–4, reviews fundamental subjects such as the band structures of semiconductors, optical transitions, optical waveguides, and optical resonators. Based on these fundamentals, the second part, Chapters 5–8, explains semiconductor lasers.

The operating principles and basic characteristics of semiconductor lasers are discussed in Chapter 5. More advanced topics, such as dynamic single-mode lasers, quantum well lasers, and control of the spontaneous emission, are described in Chapters 6–8.

Finally, the author would like to thank Professor emeritus of the University of Tokyo, Koichi Shimoda (former professor at Keio University), Professor Kiyoji Uehara of Keio University, Professor Tomoo Fujioka of Tokai University (former professor at Keio University), and Professor Minoru Obara of Keio University for their warm encouragement and precious advice since he was a student. He is also indebted to NEC Corporation, where he started research on semiconductor lasers just after graduation from Keio University. Thanks are extended to the entire team at Springer-Verlag, especially, Mr. Frank Ganz, Mr. Frank McGuckin, Ms. Margaret Mitchell, Mr. Timothy Taylor, and Dr. Hans Koelsch, for their kind help.

Takahiro Numai
Kusatsu, Japan
September 2003

Springer Series in

OPTICAL SCIENCES

New editions of volumes prior to volume 70

1 **Solid-State Laser Engineering**
By W. Koechner, 5th revised and updated ed. 1999, 472 figs., 55 tabs., XII, 746 pages

14 **Laser Crystals**
Their Physics and Properties
By A. A. Kaminskii, 2nd ed. 1990, 89 figs., 56 tabs., XVI, 456 pages

15 **X-Ray Spectroscopy**
An Introduction
By B. K. Agarwal, 2nd ed. 1991, 239 figs., XV, 419 pages

36 **Transmission Electron Microscopy**
Physics of Image Formation and Microanalysis
By L. Reimer, 4th ed. 1997, 273 figs. XVI, 584 pages

45 **Scanning Electron Microscopy**
Physics of Image Formation and Microanalysis
By L. Reimer, 2nd completely revised and updated ed. 1998,
260 figs., XIV, 527 pages

Published titles since volume 70

70 **Electron Holography**
By A. Tonomura, 2nd, enlarged ed. 1999, 127 figs., XII, 162 pages

71 **Energy-Filtering Transmission Electron Microscopy**
By L. Reimer (Ed.), 1995, 199 figs., XIV, 424 pages

72 **Nonlinear Optical Effects and Materials**
By P. Günter (Ed.), 2000, 174 figs., 43 tabs., XIV, 540 pages

73 **Evanescent Waves**
From Newtonian Optics to Atomic Optics
By F. de Fornel, 2001, 277 figs., XVIII, 268 pages

74 **International Trends in Optics and Photonics**
ICO IV
By T. Asakura (Ed.), 1999, 190 figs., 14 tabs., XX, 426 pages

75 **Advanced Optical Imaging Theory**
By M. Gu, 2000, 93 figs., XII, 214 pages

76 **Holographic Data Storage**
By H.J. Coufal, D. Psaltis, G.T. Sincerbox (Eds.), 2000
228 figs., 64 in color, 12 tabs., XXVI, 486 pages

77 **Solid-State Lasers for Materials Processing**
Fundamental Relations and Technical Realizations
By R. Iffländer, 2001, 230 figs., 73 tabs., XVIII, 350 pages

78 **Holography**
The First 50 Years
By J.-M. Fournier (Ed.), 2001, 266 figs., XII, 460 pages

79 **Mathematical Methods of Quantum Optics**
By R.R. Puri, 2001, 13 figs., XIV, 285 pages

80 **Optical Properties of Photonic Crystals**
By K. Sakoda, 2001, 95 figs., 28 tabs., XII, 223 pages

81 **Photonic Analog-to-Digital Conversion**
By B.L. Shoop, 2001, 259 figs., 11 tabs., XIV, 330 pages

82 **Spatial Solitons**
By S. Trillo, W.E. Torruellas (Eds), 2001, 194 figs., 7 tabs., XX, 454 pages

83 **Nonimaging Fresnel Lenses**
Design and Performance of Solar Concentrators
By R. Leutz, A. Suzuki, 2001, 139 figs., 44 tabs., XII, 272 pages

84 **Nano-Optics**
By S. Kawata, M. Ohtsu, M. Irie (Eds.), 2002, 258 figs., 2 tabs., XVI, 321 pages

85 **Sensing with Terahertz Radiation**
By D. Mittleman (Ed.), 2003, 207 figs., 14 tabs., XVI, 337 pages

86 **Progress in Nano-Electro-Optics I**
Basics and Theory of Near-Field Optics
By M. Ohtsu (Ed.), 2003, 118 figs., XIV, 161 pages

87 **Optical Imaging and Microscopy**
Techniques and Advanced Systems
By P. Török, F.-J. Kao (Eds.), 2003, 260 figs., XVII, 395 pages

88 **Optical Interference Coatings**
By N. Kaiser, H.K. Pulker (Eds.), 2003, 203 figs., 50 tabs., XVI, 504 pages

89 **Progress in Nano-Electro-Optics II**
Novel Devices and Atom Manipulation
By M. Ohtsu (Ed.), 2003, 115 figs., XIII, 188 pages

90/1 **Raman Amplifiers for Telecommunications 1**
Physical Principles
By M.N. Islam (Ed.), 2004, 488 figs., XXVIII, 328 pages

90/2 **Raman Amplifiers for Telecommunications 2**
Sub-Systems and Systems
By M.N. Islam (Ed.), 2004, 278 figs., XXVIII, 420 pages

91 **Optical Super Resolution**
By Z. Zalevsky, D. Mendlovic, 2004, 164 figs., XVIII, 232 pages

92 **UV-Visible Reflection Spectroscopy of Liquids**
By J.A. Räty, K.-E. Peiponen, T. Asakura, 2004, 131 figs., XII, 219 pages

93 **Fundamentals of Semiconductor Lasers**
By T. Numai, 2004, 166 figs., XII, 264 pages

94 **Photonic Crystals**
Physics, Fabrication and Applications
By K. Inoue, K. Ohtaka (Eds.), 2004, 214 figs., IX, 331 pages

Contents

1 Band Structures

1.1 Introduction

Optical transitions, such as the *emission* and *absorption* of light, are closely related to the energies of electrons, as shown in Table 1.1. When electrons transit from high energy states to lower ones, lights are emitted, and in the reverse process, lights are absorbed. Note that *nonradiative transitions*, which do not emit lights, also exist when electrons transit from high energy states to lower ones. Light emissions, however, always accompany the transitions of electrons from high energy states to lower ones, which are referred to as *radiative transitions*.

Table 1.1. Relationship between electron energies and optical transitions

Energy of the Electrons	Optical Transition
High → low	Emission
Low → high	Absorption

Let us consider electron energies, which are the bases of the optical transitions. Figure 1.1 shows a relationship between atomic spacing and electron energies. When the atomic spacing is large, such as in gases, the electron energies are *discrete* and the *energy levels* are formed. With a decrease in the atomic spacing, the wave functions of the electrons start to overlap. Therefore, the energy levels begin to split so as to satisfy the *Pauli exclusion principle*. With an increase in the number of neighboring atoms, the number of split energy levels is enhanced, and the energy differences in the adjacent energy levels are reduced. In the semiconductor crystals, the number of atoms per cubic centimeter is on the order of 10^{22}, where the lattice constant is approximately 0.5 nm and the atomic spacing is about 0.2 nm. As a result, the spacing of energy levels is on the order of 10^{-18} eV. This energy spacing is much smaller than the *bandgap*, which is on the order of electron volts. Therefore, the constituent energy levels, which are known as the *energy bands*, are considered to be almost *continuous*.

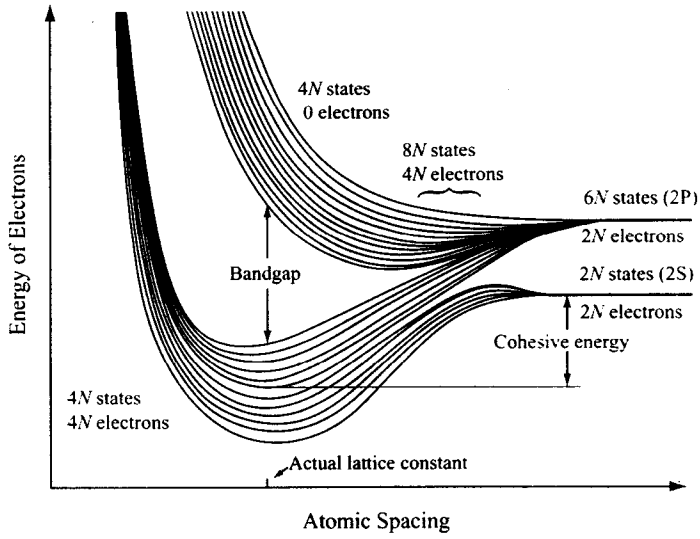

Fig. 1.1. Relationship between atomic spacing and electron energies for the diamond structure with N atoms

1.2 Bulk Structures

1.2.1 $k \cdot p$ Perturbation Theory

We study the band structures of the *bulk* semiconductors, in which constituent atoms are periodically placed in a sufficiently long range compared with the lattice spacing.

Semiconductors have carriers, such as free electrons and holes, only in the vicinity of the band edges. As a result, we would like to know the band shapes and the effective masses of the carriers near the band edges, and they often give us enough information to understand fundamental characteristics of the optical transitions. When we focus on the neighbor of the band edges, it is useful to employ the ***k·p perturbation theory*** [1–4] whose *wave vectors* $\boldsymbol{k}$s are near the band edge wave vector $\boldsymbol{k}_0$ inside the *Brillouin zone*. The *wave functions* and *energies* of the bands are calculated with $\Delta\boldsymbol{k} = \boldsymbol{k} - \boldsymbol{k}_0$ as a *perturbation parameter*. For brevity, we put $\boldsymbol{k}_0 = 0$ in the following.

The *Schrödinger equation* in the steady state is written as [5, 6]

$$\left[-\frac{\hbar^2}{2m}\nabla^2 + V(\boldsymbol{r})\right]\psi_{n\boldsymbol{k}}(\boldsymbol{r}) = E_n(\boldsymbol{k})\psi_{n\boldsymbol{k}}(\boldsymbol{r}), \tag{1.1}$$

where $\hbar = h/2\pi = 1.0546 \times 10^{-34}\,\mathrm{J\,s}$ is *Dirac's constant*, $h = 6.6261 \times 10^{-34}\,\mathrm{J\,s}$ is *Planck's constant*, $m = 9.1094 \times 10^{-31}\,\mathrm{kg}$ is the electron mass in a vacuum, $V(\boldsymbol{r})$ is a potential, $\psi_{n\boldsymbol{k}}(\boldsymbol{r})$ is a wave function, $E_n(\boldsymbol{k})$ is an *energy eigenvalue*, n is a *quantum number*, and $\boldsymbol{k}$ is a wave vector. In the *single crystals* where the atoms are placed *periodically*, the potential $V(\boldsymbol{r})$ is

spatially periodic. Therefore, as a solution of (1.1), we can consider the *Bloch function* given by

$$\psi_{n\boldsymbol{k}}(\boldsymbol{r}) = \mathrm{e}^{\mathrm{i}\boldsymbol{k}\cdot\boldsymbol{r}} u_{n\boldsymbol{k}}(\boldsymbol{r}), \tag{1.2}$$

$$u_{n\boldsymbol{k}}(\boldsymbol{r}) = u_{n\boldsymbol{k}}(\boldsymbol{r}+\boldsymbol{R}), \tag{1.3}$$

where $\boldsymbol{R}$ is a vector indicating the periodicity of the crystal. Equations (1.2) and (1.3) are called the *Bloch theorem*, which indicates that the wave function $u_{n\boldsymbol{k}}(\boldsymbol{r})$ depends on the wave vector $\boldsymbol{k}$ and has the same periodicity as that of the crystal. Substituting (1.2) into (1.1) results in

$$\left[-\frac{\hbar^2}{2m}\nabla^2 + V(\boldsymbol{r}) + \mathcal{H}'\right] u_{n\boldsymbol{k}}(\boldsymbol{r}) = E_n(\boldsymbol{k}) u_{n\boldsymbol{k}}(\boldsymbol{r}), \tag{1.4}$$

where

$$\mathcal{H}' = \frac{\hbar^2\boldsymbol{k}^2}{2m} + \frac{\hbar}{m}\boldsymbol{k}\cdot\boldsymbol{p}, \tag{1.5}$$

$$\boldsymbol{p} = -\mathrm{i}\hbar\nabla. \tag{1.6}$$

In the $\boldsymbol{k}\cdot\boldsymbol{p}$ perturbation theory, which is only valid for small $\boldsymbol{k}$, we solve (1.4) by regarding (1.5) as the *perturbation*. Note that the name of the $\boldsymbol{k}\cdot\boldsymbol{p}$ perturbation stems from the second term on the right-hand side of (1.5).

When we consider the energy band with $n = 0$, the wave equation for the unperturbed state with $\boldsymbol{k} = 0$ is expressed as

$$\left[-\frac{\hbar^2}{2m}\nabla^2 + V(\boldsymbol{r})\right] u_{00}(\boldsymbol{r}) = E_0(0) u_{00}(\boldsymbol{r}). \tag{1.7}$$

In the following, for simplicity, the wave function $u_{n\boldsymbol{k}}(\boldsymbol{r})$ and the energy $E_0(0)$ are represented as $u_n(\boldsymbol{k},\boldsymbol{r})$ and E_0, respectively.

At first, we consider a nondegenerate case, in which the energy of the state n is always different from that of the other state n' ($\neq n$). From the *first-order perturbation theory* (see Appendix B), the wave function $u_0(\boldsymbol{k},\boldsymbol{r})$ is given by

$$u_0(\boldsymbol{k},\boldsymbol{r}) = u_0(0,\boldsymbol{r}) + \sum_{\alpha\neq 0} \frac{-\mathrm{i}\,(\hbar^2/m)\boldsymbol{k}\cdot\langle\alpha|\nabla|0\rangle}{E_0 - E_\alpha} u_\alpha(0,\boldsymbol{r}), \tag{1.8}$$

$$\langle\alpha|\nabla|0\rangle = \int u_\alpha{}^*(0,\boldsymbol{r})\nabla u_0(0,\boldsymbol{r})\,\mathrm{d}^3\boldsymbol{r}, \tag{1.9}$$

where $u_n(\boldsymbol{k},\boldsymbol{r})$ is assumed to be an orthonormal function. Here, $\langle\alpha|$ and $|0\rangle$ are the *bra vector* and the *ket vector*, respectively, which were introduced by Dirac. In the *second-order perturbation theory*, an energy eigenvalue is obtained as

$$E(\boldsymbol{k}) = E_0 + \frac{\hbar^2 k^2}{2m} + \frac{\hbar^2}{m^2}\sum_{i,j} k_i k_j \sum_{\alpha\neq 0} \frac{\langle 0|p_i|\alpha\rangle\langle\alpha|p_j|0\rangle}{E_0 - E_\alpha}. \tag{1.10}$$

From (1.10), the *reciprocal effective mass tensor* is defined as

$$\left(\frac{1}{m}\right)_{ij} \equiv \frac{1}{\hbar^2}\frac{\partial^2 E}{\partial k_i \partial k_j} = \frac{1}{m}\left(\delta_{ij} + \frac{2}{m}\sum_{\alpha\neq 0}\frac{\langle 0|p_i|\alpha\rangle\langle\alpha|p_j|0\rangle}{E_0 - E_\alpha}\right). \tag{1.11}$$

With the help of (1.11), (1.10) reduces to

$$E(\boldsymbol{k}) = E_0 + \frac{\hbar^2}{2}\sum_{i,j}\left(\frac{1}{m}\right)_{ij} k_i k_j. \tag{1.12}$$

This equation includes the periodicity of the crystal (potential) in the mass of the electron as the effective mass. This effective mass is useful to make analysis easier. For example, in the quantum well (QW) structures, the electrons see both the periodic potential of the crystal and the quantum well potential. If we express equations using the effective mass, we have only to consider the quantum well potential, because the periodic potential of the crystal is already included in the effective mass. This approximation is referred to as the *effective mass approximation.*

In the following, we will consider the band structures of semiconductor crystals. Most semiconductor crystals for semiconductor lasers have a *zinc-blende structure*, in which the bottom of the conduction bands is *s*-orbital-like and the tops of the valence bands are *p*-orbital-like. In zinc-blende or diamond structures, the atomic bonds are formed via sp^3 ***hybrid orbitals*** as follows:

$$\begin{aligned}
&\mathrm{C} : (2s)^2(2p)^2 \rightarrow (2s)^1(2p)^3 \\
&\mathrm{Si} : (3s)^2(3p)^2 \rightarrow (3s)^1(3p)^3 \\
&\mathrm{ZnS} : \mathrm{Zn} : (3d)^{10}(4s)^2 \rightarrow \mathrm{Zn}^{2-} : (3d)^{10}(4s)^1(4p)^3 \\
&\qquad\quad \mathrm{S} : (3s)^2(3p)^4 \rightarrow \mathrm{S}^{2+} : (3s)^1(3p)^3
\end{aligned}$$

Therefore, the wave functions for the electrons in the zinc-blende or diamond structures are expressed as superpositions of the *s*-orbital function and *p*-orbital functions.

Let us calculate the wave functions and energies of the bands in the zinc-blende structures. We assume that both the bottom of the conduction band and the tops of the valence bands are placed at $\boldsymbol{k} = 0$, as in the direct transition semiconductors, which will be elucidated in Section 2.1. When the spin-orbit interaction is neglected, the tops of the valence bands are three-fold *degenerate* corresponding to the three *p*-orbitals (p_x, p_y, p_z). Here, the wave functions are written as

the *s*-orbital function for the bottom of the conduction band : $u_s(\boldsymbol{r})$,
the *p*-orbital functions for the tops of the valence bands :
$u_x = xf(\boldsymbol{r})$, $u_y = yf(\boldsymbol{r})$, $u_z = zf(\boldsymbol{r})$, $f(\boldsymbol{r})$: a spherical function.

When the energy bands are degenerate, a perturbed wave equation is given by a linear superposition of $u_s(\boldsymbol{r})$ and $u_j(\boldsymbol{r})$ $(j = x, y, z)$ as

$$u_n(\boldsymbol{k}, \boldsymbol{r}) = Au_s(\boldsymbol{r}) + Bu_x(\boldsymbol{r}) + Cu_y(\boldsymbol{r}) + Du_z(\boldsymbol{r}), \tag{1.13}$$

where A, B, C, and D are coefficients.

To obtain the energy eigenvalues, we rewrite (1.4) as

$$\left[-\frac{\hbar^2}{2m}\nabla^2 + V(\boldsymbol{r}) + \mathcal{H}'_{\rm d}\right] u_n(\boldsymbol{k}, \boldsymbol{r}) = \left[E_n(\boldsymbol{k}) - \frac{\hbar^2 k^2}{2m}\right] u_n(\boldsymbol{k}, \boldsymbol{r}), \tag{1.14}$$

$$\mathcal{H}'_{\rm d} = \frac{\hbar}{m}\,\boldsymbol{k}\cdot\boldsymbol{p} = -\frac{\mathrm{i}\hbar^2}{m}\boldsymbol{k}\cdot\nabla. \tag{1.15}$$

Note that the unperturbed equation is obtained by setting $\boldsymbol{k} = 0$ in (1.14), where $E_n(0) = E_{\rm c}$ and $u_0(0, \boldsymbol{r}) = u_s(\boldsymbol{r})$ for the conduction band, while $E_n(0) = E_{\rm v}$ and $u_0(0, \boldsymbol{r}) = u_j(\boldsymbol{r})$ $(j = x, y, z)$ for the valence bands. Here, $E_{\rm c}$ is the energy of the bottom of the conduction band, and $E_{\rm v}$ is the energy of the tops of the valence bands.

Substituting (1.13) into (1.14); multiplying ${u_s}^*(\boldsymbol{r})$, ${u_x}^*(\boldsymbol{r})$, ${u_y}^*(\boldsymbol{r})$, and ${u_z}^*(\boldsymbol{r})$ from the left-hand side; and then integrating with respect to a volume over the space leads to

$$\begin{aligned}
&(\mathcal{H}'_{ss} + E_{\rm c} - \lambda)A + \mathcal{H}'_{sx}B + \mathcal{H}'_{sy}C + \mathcal{H}'_{sz}D = 0,\\
&\mathcal{H}'_{xs}A + (\mathcal{H}'_{xx} + E_{\rm v} - \lambda)B + \mathcal{H}'_{xy}C + \mathcal{H}'_{xz}D = 0,\\
&\mathcal{H}'_{ys}A + \mathcal{H}'_{yx}B + (\mathcal{H}'_{yy} + E_{\rm v} - \lambda)C + \mathcal{H}'_{yz}D = 0,\\
&\mathcal{H}'_{zs}A + \mathcal{H}'_{zx}B + \mathcal{H}'_{zy}C + (\mathcal{H}'_{zz} + E_{\rm v} - \lambda)D = 0,
\end{aligned} \tag{1.16}$$

where

$$\begin{aligned}
\mathcal{H}'_{ij} &= \langle u_i|\mathcal{H}'_{\rm d}|u_j\rangle = \int {u_i}^*(\boldsymbol{r})\mathcal{H}'_{\rm d}u_j(\boldsymbol{r})\,\mathrm{d}^3\boldsymbol{r} \quad (i, j = s, x, y, z),\\
\lambda &= E_n(\boldsymbol{k}) - \frac{\hbar^2 k^2}{2m}.
\end{aligned} \tag{1.17}$$

Note that the orthonormality of $u_s(\boldsymbol{r})$ and $u_j(\boldsymbol{r})$ $(j = x, y, z)$ were used to derive (1.16).

In (1.16), only when the determinant for the coefficients A, B, C, and D is zero, we have solutions A, B, C, and D other than $A = B = C = D = 0$. From (1.16) and (1.17), the determinant is given by

$$\begin{vmatrix}
E_{\rm c} - \lambda & Pk_x & Pk_y & Pk_z\\
P^*k_x & E_{\rm v} - \lambda & 0 & 0\\
P^*k_y & 0 & E_{\rm v} - \lambda & 0\\
P^*k_z & 0 & 0 & E_{\rm v} - \lambda
\end{vmatrix} = 0, \tag{1.18}$$

$$P = -\mathrm{i}\frac{\hbar^2}{m}\int {u_s}^*\frac{\partial u_j}{\partial r_j}\,\mathrm{d}^3\boldsymbol{r}, \quad P^* = -\mathrm{i}\frac{\hbar^2}{m}\int {u_j}^*\frac{\partial u_s}{\partial r_j}\,\mathrm{d}^3\boldsymbol{r} \tag{1.19}$$

$$(j = x, y, z, \quad r_x = x, \ r_y = y, \ r_z = z).$$

The solutions of (1.18) are obtained as

$$E_{1,2}(\boldsymbol{k}) = \frac{E_c + E_v}{2} + \frac{\hbar^2 k^2}{2m} \pm \left[\left(\frac{E_c - E_v}{2} \right)^2 + k^2 |P|^2 \right]^{1/2}, \tag{1.20}$$

$$E_{3,4}(\boldsymbol{k}) = E_v + \frac{\hbar^2 k^2}{2m}, \tag{1.21}$$

where (1.17) was used. Figure 1.2 shows the calculated results of (1.20) and (1.21). It should be noted that the spin-orbit interaction has been neglected and only the first-order perturbation has been included to derive these equations.

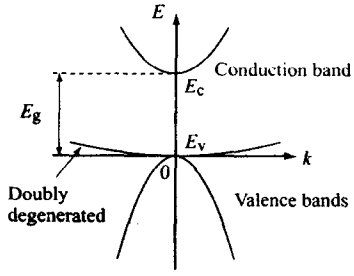

Fig. 1.2. Energy of the conduction and valence bands. Here, only the first-order perturbation is included; the spin-orbit interaction is neglected

1.2.2 Spin-Orbit Interaction

We consider the band structures by introducing the spin-orbit interaction and the second-order perturbation. First, let us treat the *spin-orbit interaction* semiclassically. As shown in Fig. 1.3, the electron with the electric charge $-e = -1.6022 \times 10^{-19}$ C rotates about the nucleus with the electric charge $+Ze$. The velocity of the electron is $\boldsymbol{v}$, and the distance between the electron and the nucleus is $|\boldsymbol{r}|$.

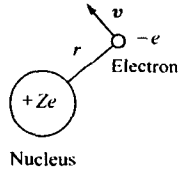

Fig. 1.3. Motions of the electron

If the origin of the reference system is placed at the electron, the nucleus seems to rotate about the electron with the velocity $-\boldsymbol{v}$. As a result, due

to *Biot-Savart's law*, a *magnetic flux density* $\boldsymbol{B}$ is produced at the electron, which is written as

$$\boldsymbol{B} = \frac{\mu_0}{4\pi} Ze \frac{\boldsymbol{r} \times \boldsymbol{v}}{r^3} = \frac{\mu_0}{4\pi} \frac{Ze}{m} \frac{1}{r^3} \boldsymbol{l}. \tag{1.22}$$

Here, μ_0 is magnetic permeability in a vacuum, and $\boldsymbol{l}$ is the *orbital angular momentum* given by

$$\boldsymbol{l} = \boldsymbol{r} \times \boldsymbol{p} = \boldsymbol{r} \times m\boldsymbol{v}. \tag{1.23}$$

The *spin magnetic moment* $\boldsymbol{\mu}_\mathrm{s}$ is expressed as

$$\boldsymbol{\mu}_\mathrm{s} = -\frac{e}{m}\boldsymbol{s} = -\frac{2\mu_\mathrm{B}}{\hbar}\boldsymbol{s}, \tag{1.24}$$

where $\boldsymbol{s}$ is the *spin angular momentum* and μ_B is the *Bohr magneton* defined as

$$\mu_\mathrm{B} \equiv \frac{e\hbar}{2m} = 9.2732 \times 10^{-24}\,\mathrm{A\,m^2}. \tag{1.25}$$

As a result, the *interaction energy* $\mathcal{H}_\mathrm{SO}$ between the *spin magnetic moment* $\boldsymbol{\mu}_\mathrm{s}$ and the magnetic flux density $\boldsymbol{B}$ is obtained as

$$\mathcal{H}_\mathrm{SO} = -\boldsymbol{\mu}_\mathrm{s} \cdot \boldsymbol{B} = \frac{\mu_0}{4\pi} \frac{Ze^2}{m^2} \frac{1}{r^3} \boldsymbol{l} \cdot \boldsymbol{s}. \tag{1.26}$$

From Dirac's *relativistic quantum mechanics*, the interaction energy $\mathcal{H}_\mathrm{SO}$ is given by

$$\mathcal{H}_\mathrm{SO} = \frac{\mu_0}{4\pi} \frac{Ze^2}{2m^2} \frac{1}{r^3} \boldsymbol{l} \cdot \boldsymbol{s}, \tag{1.27}$$

which is half of (1.26). As explained earlier, the spin-orbit interaction generates a magnetic field at the electron due to the orbital motions of the nucleus, and this field interacts with the electron's spin magnetic moment.

Introducing *Pauli's spin matrices* $\boldsymbol{\sigma}$ such as

$$\boldsymbol{s} = \frac{\hbar}{2}\boldsymbol{\sigma}, \tag{1.28}$$

$$\sigma_x = \begin{bmatrix} 0 & 1 \\ 1 & 0 \end{bmatrix}, \quad \sigma_y = \begin{bmatrix} 0 & -\mathrm{i} \\ \mathrm{i} & 0 \end{bmatrix}, \quad \sigma_z = \begin{bmatrix} 1 & 0 \\ 0 & -1 \end{bmatrix}, \tag{1.29}$$

we can write the *spin-orbit interaction Hamiltonian* $\mathcal{H}_\mathrm{SO}$ as

$$\mathcal{H}_\mathrm{SO} = \frac{\mu_0}{4\pi} \frac{Ze^2}{2m^2} \frac{1}{r^3} \frac{\hbar}{2} \boldsymbol{l} \cdot \boldsymbol{\sigma}. \tag{1.30}$$

If we express the *up-spin* $\uparrow$ $(s_z = \hbar/2)$ as α and the *down-spin* $\downarrow$ $(s_z = -\hbar/2)$ as β, they are written in matrix form as